Three-Dimensional Strongly Coupled Plasma Crystal under Gravity Conditions

M. Zuzic,[1,*] A. V. Ivlev,[1] J. Goree,[2] G. E. Morfill,[1] H. M. Thomas,[1] H. Rothermel,[1] U. Konopka,[1] R. Sütterlin,[1] and D. D. Goldbeck[1]

[1]*Max-Planck-Institut für Extraterrestrische Physik, D-85740 Garching, Germany*
[2]*Department of Physics and Astronomy, The University of Iowa, Iowa City, Iowa 52242*
(Received 9 May 2000)

Experiments were carried out to investigate a three-dimensional (3D) plasma crystal. A method of determining the positions of each individual microparticle has been developed. A crystal volume of about 2×10^4 particles in 19 horizontal planes was analyzed. Direct imaging and the 3D pair correlation function show that "domains" of fcc and hcp lattices coexist in the crystal. Other structures, in particular, the theoretically predicted bcc lattice, were not observed.

PACS numbers: 52.25.Zb, 52.25.Ub

Since 1994, when "plasma crystals" were observed for the first time in experiments [1–3], there have been a number of studies of crystal structure and phase transitions; see, e.g., [4]. Most of the experiments were performed in radio-frequency (rf) discharges, where the micron sized particles are levitated in the electric field of the lower electrode sheath in ordered structures with one or a few horizontal particle layers. Three-dimensional (3D) crystals were also observed in some experiments, where the particles order themselves in fcc, bcc, and hcp lattices, as well as string-like structures [5–7].

In this Letter, we report measurements of a plasma crystal with 19 horizontal lattice planes (layers). We imaged a volume with about 2×10^4 microspheres, which is more than in previous reports (see, e.g., [5]). From the images, we identify the xyz coordinates of all the particles in the sample volume using a technique that we devised. Analysis of the individual particle positions shows that the crystal contains regions of either fcc or hcp lattices, distributed in different domains and separated by a transition region typically 2–3 lattice planes wide. The particle coordinates are then used not only to identify the local crystalline lattice type, but also to measure the three-dimensional pair correlation function. We determine the volume ratio of the two lattice structures coexisting in the crystal sample, which allows us to make a comparison with results of molecular dynamics simulations [8].

The experiments were performed in a symmetrically driven directly coupled rf chamber. The same setup was used earlier in parabola and rocket flights in order to investigate the behavior of "complex plasmas" under microgravity conditions [9]. The term complex plasma refers to composition (ions, electrons, charged microspheres) in analogy to the term "complex fluids" in colloids [10]. Polymer microparticles of melamine formaldehyde with a diameter of 3.375 ± 0.102 μm were injected through a dispenser into an argon plasma at a pressure of 0.47 mbar. The peak-to-peak rf voltage on the lower electrode was 61.8 V.

To measure the 3D structure (z corresponds to the vertical direction and xy is the horizontal plane) a vertical laser sheet of $\simeq 160$ μm thickness, parallel to the xz plane, moves in the y direction over a distance of 5.5 mm with a constant velocity $v = 0.30$ mm/s. The duration of the whole scan is about 18 s. The particles are imaged from the side (in the y direction) by an external charge-coupled device (CCD) camera. The camera moves together with the laser sheet in order to keep the particles in focus [5]. Images were recorded 15 min after particle injection, to allow the lattice to anneal. The crystallization started from the bottom.

In order to determine the particle positions in 3D, a set of consecutive video frames (full frame rate $1/\tau = 25$ frames/s, resolution 768×576 pixels/frame, 8 bit gray scale steps) is digitized. Each particle is represented on a video frame by a light spot with an intensity distribution $I_i(x, z)$. An intensity threshold I_{th} is chosen to identify a particle from background fluctuations. We set $I_i = 0$ when $I_i < I_{\text{th}}$. Then the coordinates of the ith particle on the frame are $\{X_i, Z_i\} = \int\{x, z\} I_i(x, z)\, dx\, dz / \int I_i(x, z)\, dx\, dz$. To measure the third coordinate Y_i, we calculate the mean intensity of the ith particle for each consecutive frame. For the nth frame, the mean intensity is $\tilde{I}_i(n) = \int I_i(x, z)\, dx\, dz / \int dx\, dz$. Then $Y_i = N_i v \tau$, where $N_i = \sum n \tilde{I}_i(n) / \sum \tilde{I}_i(n)$. The particle coordinates in a frame, $\{X_i, Z_i\}$, have an error of one pixel or better ($\lesssim 9$ μm), the error of Y_i is about $v\tau/2 \simeq 6$ μm. The thermal motion of the particles around their equilibrium position is small, with a mean amplitude of less than one pixel.

Using the measured 3D coordinates we found that the horizontal interparticle distance Δ_{xy} decreases $\simeq 40\%$ from top to bottom as shown in Fig. 1. We attribute this to the compression by the gravitational force. The particle number per unit length in the vertical z direction as well as the total number of particles in each horizontal layer is shown in Fig. 2. The distribution of particles in each layer is rather narrow, so that we can easily distinguish neighboring planes. Figure 3 shows that the thickness of layers

 0031-9007/00/85(19)/4064(4)$15.00

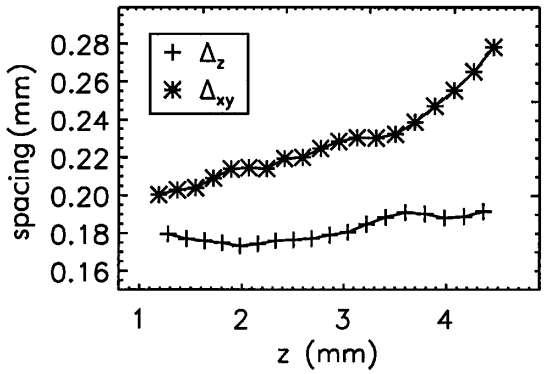

FIG. 1. Vertical distance (+) between the horizontal planes, Δ_z, and the mean interparticle distance (*) in each plane, Δ_{xy}, as functions of vertical position z.

also decreases towards the bottom. Thus, layers become compressed by the weight of the particles above, and the intergrain coupling in each layer increases. This leads to a high ordering of particles in the lower and medium layers [see Figs. 3(b) and 3(c)] with just a few dislocations. Particles in the upper layer are not subjected to "pressure" from above and therefore are more disordered [see Fig. 3(a)]. The particle charge variation with height can also influence the ordering. Note that the interplane distance, Δ_z, varies rather slowly in the z direction, and that $\Delta_z(z)$ attains a minimum in the lower part of the crystal (see Fig. 1). This behavior of $\Delta_z(z)$ can be understood if we consider the force balance on a particle suspended in a certain layer. The difference of the gravity, Mg, and electrostatic, QE_{sh}, forces is equalized by the difference of the forces acting on the particle from the layers below, F_{down}, and above, F_{up}, the considered layer: $Mg - QE_{\mathrm{sh}} = F_{\mathrm{down}} - F_{\mathrm{up}}$. We assume that the particles interact via the screened Coulomb potential and only the nearest-neighbor interaction is essential (see discussion below), so that the interparticle force F is a rapidly decreasing function of Δ_z. In the upper part of the crystal, where the electric field of the sheath, E_{sh}, is weak we have $F_{\mathrm{down}} - F_{\mathrm{up}} > 0$, and therefore the separation Δ_z increases with z. In the bottom part of the crystal the opposite inequality is satisfied and thus Δ_z decreases with z. The minimum is attained in the region where $Mg \sim QE_{\mathrm{sh}}$. The effect of gravitational compression can also be seen in Fig. 3 of Juan *et al.* [11] where particles were confined by a parabolic potential well, and gravity applied a tangential force.

In order to identify different possible lattice types in the plasma crystal, small volumes of uniform structure were investigated. We sequentially superimposed 2D images of each triplet of adjacent horizontal layers. Only two types of symmetry (and their mixture) are found to coexist in the crystal, and Fig. 4 illustrates them. The particle positions of three consecutive layers are marked in green (A), blue (B), and red (C). Comparison with ideal lattices shows that the sample in Fig. 4(a) is an hcp lattice [12]. The sample in Fig. 4(b) corresponds either to a fcc or bcc type with the (111) lattice plane parallel to the electrode (horizontal plane xy). These two lattices look the same perpendicular to the (111) plane. However, the distance between adjacent layers is different: Δ_z is larger for fcc by a factor of $\simeq 2.5$ (for equal Δ_{xy}). Since Δ_z is nearly constant and Δ_{xy} varies

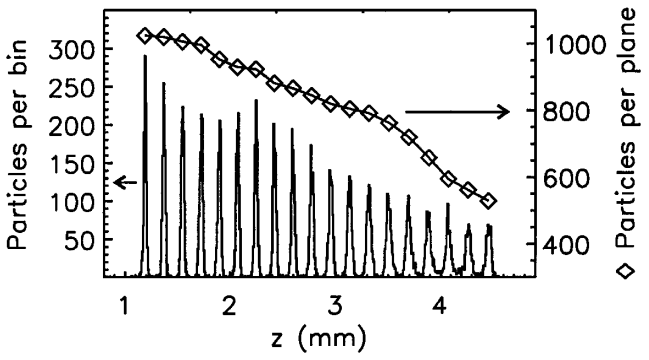

FIG. 2. Density of particles along the vertical z axis (particle number per bin of 8 μm size, solid line), and number of particles in each lattice plane (◇).

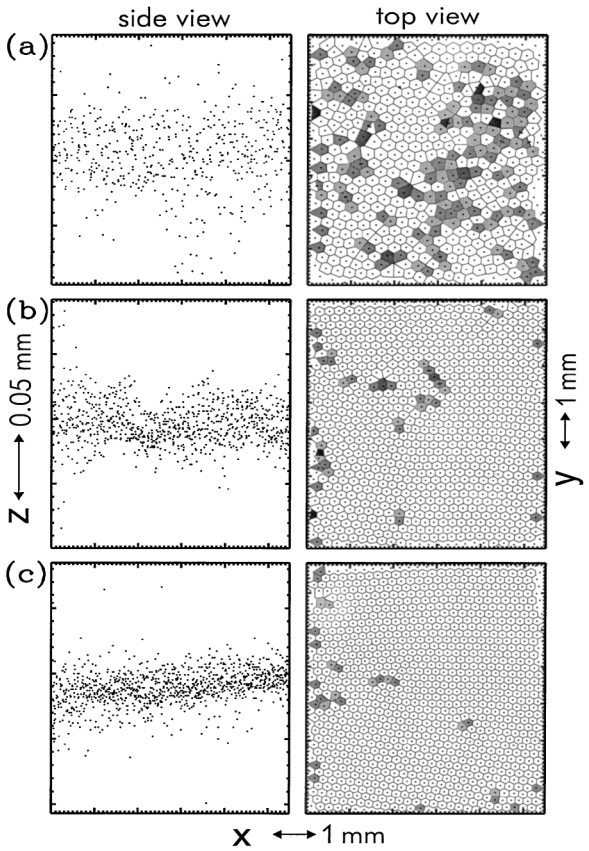

FIG. 3. Upper (nineteenth) plane (a), middle (ninth) plane (b), and the lower (first) plane (c) of the crystal. The left and right columns show the side and top views of the planes, respectively. In the top view, four-, five-, seven- and eightfold lattice cells are marked by different gray scales; the rest of the structure is hexagonal, except at the boundaries.

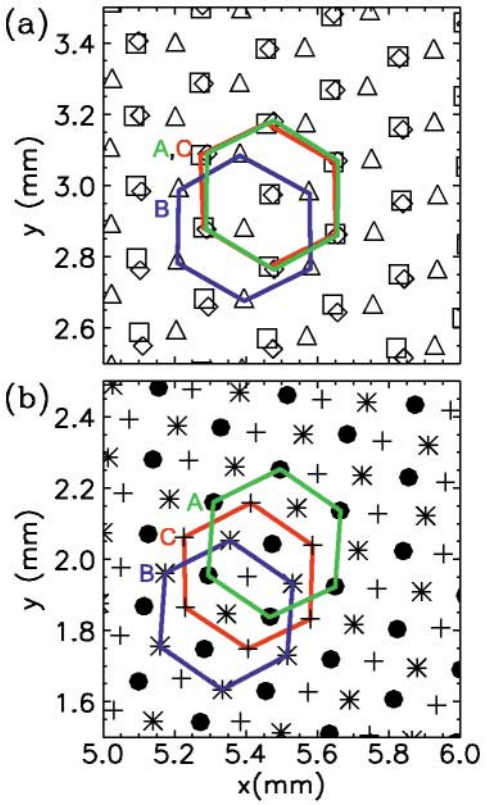

FIG. 4 (color). Top view on three superimposed crystal layers near the bottom of the crystal. The fourth (□), fifth (△), and the sixth (◇) layers counting from the bottom are hcp [see (a)]. The first (•), second (∗), and the third (+) layers in (b) are either fcc or bcc, with the (111) plane parallel to the electrodes.

only within ≃40%, there are two possibilities: the whole crystal is a mixture of either hcp and bcc, or hcp and fcc phases. The simplest way to determine which case we have is to rotate the sample in Fig. 4(b) from the (111) to the (001) orientation. The top view of the sample ($x'y'$ plane) is then shown in Fig. 5. We see that the structure corresponds to the fcc lattice [12]. Thus we conclude that the plasma crystal consists of pure fcc and hcp lattice zones with some transitional regions in between. An example of this coexistence is presented in Fig. 6. This top view of the three adjacent layers is typical for the whole crystal (excluding a few upper layers, where particles are more disordered). One can see that the fcc and hcp regions are distributed in domains and that the transition from one domain to the next requires about two lattices. Analyzing the whole crystal in this way, we evaluate the volume fraction of fcc to hcp phases as $3/2$.

Note that vertical stringlike structures (when particles are aligned in vertical chains) do not exist in this crystal. Such structures are very prominent in plasma crystals with few horizontal planes and those consisting of large particles (about 7 μm or more, e.g., [13]). The reason for the alignment is believed to be the focusing of the ion flow in the plasma sheath [14], causing a lower particle to be trapped in the region of excessive positive charge in the

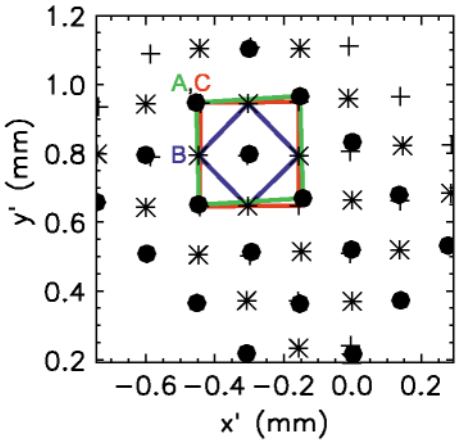

FIG. 5 (color). Determination of the lattice type seen in Fig. 4(b): The region of undefined lattice type (fcc or bcc) rotated from the (111) plane (xy) to the (001) plane ($x'y'$) is shown. We see that the particles in the first (•), second (∗), and third (+) planes form a fcc lattice.

wake of the upper one. Ion focusing is weaker for smaller particles (both because their charge is smaller, and because they levitate in the presheath due to their smaller weight, where the ion velocity is less. A higher gas pressure such as ours also weakens the focusing due to ion scattering on neutrals [14].

The absence of vertical alignment in the experiment indicates that the effects of ion flow on the interparticle potential are weak. The experiment of Konopka *et al.* [15] demonstrated that for a particle in a sheath, the interparticle potential in the horizontal direction is accurately modeled by the Yukawa potential. In that case, the effect of ion flow was insignificant, because the potential was measured in the orthogonal direction. Therefore, it is reasonable to assume that in any experiment where ion flow has an insignificant effect on the interparticle potential, the Yukawa potential will accurately model the experiment. Numerical simulations of the phase transitions in Yukawa

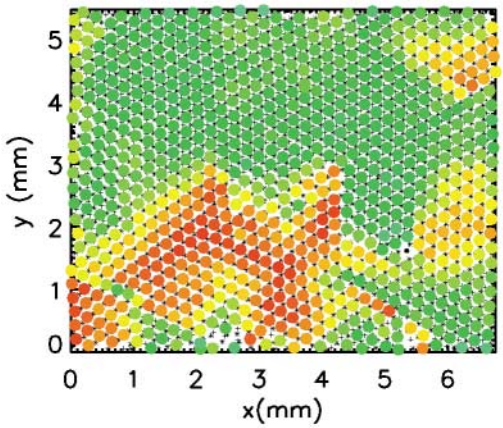

FIG. 6 (color). Coexistence of fcc (red) and hcp (green) lattices in the middle of the crystal (from eighth to tenth horizontal layers).

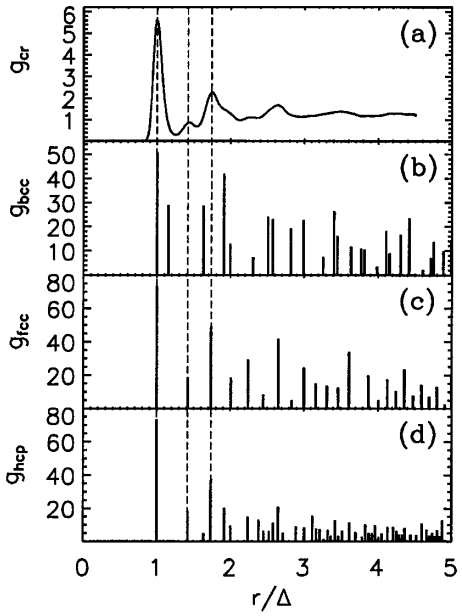

FIG. 7. 3D correlation function of the crystal, $g_{cr}(r)$, averaged over the observed space (a), and the correlation functions for different ideal lattice types: bcc (b), fcc (c), and hcp (d).

systems [8] predict a transition from bcc to fcc in the case of a strong screening, when the parameter $\kappa = \Delta/\lambda$ exceeds unity (Δ is the mean interparticle distance and λ is the screening length of the interaction). At the same time, the coupling parameter $\Gamma = Q^2/\Delta T$, where T is the temperature, must be sufficiently large for crystallization. The absence of a bcc phase in our experiments suggests that the interparticle coupling in the crystal is strongly screened, $\kappa \gtrsim 1-2$.

A transition between fcc and hcp phases has never been considered in Yukawa simulations, because both the coupling (Madelung) energy $E(\kappa)$, and the harmonic entropy constant $\Sigma(\kappa)$, for the fcc lattice are always smaller than those for the hcp lattice [16]. Thus, the Helmholtz free energy (per particle, normalized to T), $f = E(\kappa)\Gamma + \Sigma(\kappa)$, is smaller for the fcc lattice, and hence this is the thermodynamically preferred state. However, for $\kappa \gtrsim 1$ the free energies of fcc and hcp phases should converge rapidly as κ increases. This is because the nearest-neighbor configurations of both lattices are exactly the same, and only the next "shell" of surrounding particles can slightly change the value of f. Small local fluctuations of the particle density, charge, or temperature might result in a transition from the fcc to the hcp phase in this case, and the hcp/fcc volume fraction should increase with κ and tend to $1/1$ for $\kappa \gg 1$. Taking into account the value of this fraction in our experiment (2/3), we again conclude that κ might be of the order of "a few" in our crystal. To obtain a crystalline state, the coupling parameter should then be very large, $\Gamma \gtrsim 10^3-10^4$, because the fluid-solid phase transition observed in simulations in the limit of strong screening is approximated by the parameter $\Gamma^* = \Gamma e^{-\kappa}$ [8].

The average overall crystal structure can also be determined from the translational pair correlation function, $g_{cr}(r)$, which we computed in 3D, as shown in Fig. 7(a). The variation of the lattice distances with height leads to the observed broadening of the peaks. We compare $g(r)$ for ideal lattices with $g_{cr}(r)$ in Fig. 7. From the position of the first peak of $g_{cr}(r)$ a mean lattice spacing of the whole system is found to be $\Delta \simeq 215$ μm. The radial positions of the second and third peak are marked to distinguish the structures observed in the experiment. We see that the positions and the magnitude ratios of the first three peaks for fcc and hcp lattices are well correlated with the peaks of g_{cr}. Meanwhile, a bcc lattice [see Fig. 7(b)] can be ruled out, because its second and third peaks are obviously uncorrelated with g_{cr}.

To summarize, we performed first experiments to investigate "substantial" 3D laboratory plasma crystals (about 2×10^4 particles). Analysis of the particle positions shows that different domains of fcc and hcp lattices coexist in the crystal. We do not observe either the bcc phase or the vertical particle alignment, which is usually seen in $2\frac{1}{2}$D crystals. The transitions between fcc and hcp are probably caused by slight particle density, charge, or temperature variations; however, this still awaits experimental confirmation.

This work was supported by the German Aerospace Research Center DLR, Contract No. 50 WM 98520. J. G. was supported by NASA and the NSF.

*Electronic address: zuzic@mpe.mpg.de

[1] H. Thomas *et al.,* Phys. Rev. Lett. **73**, 652 (1994).
[2] J. H. Chu and Lin I, Phys. Rev. Lett. **72**, 4009 (1994).
[3] Y. Hayashi and K. Tachibana, Jpn. J. Appl. Phys. **33**, L804 (1994).
[4] H. M. Thomas and G. Morfill, Nature (London) **379**, 806 (1996).
[5] J. B. Pieper, J. Goree, and R. A. Quinn, Phys. Rev. E **54**, 5636 (1996).
[6] J. H. Chu and Lin I, Physica (Amsterdam) **205A**, 183 (1994).
[7] Y. Hayashi, Phys. Rev. Lett. **83**, 4764 (1999).
[8] S. Hamaguchi, R. T. Farouki, and D. H. E. Dubin, Phys. Rev. E **56**, 4671 (1997).
[9] G. E. Morfill *et al.,* Phys. Rev. Lett. **83**, 1598 (1999).
[10] D. Samsonov *et al.,* Phys. Rev. E **61**, 5557 (2000).
[11] W.-T. Juan, Z.-H. Huang, J.-W. Hsu, Y.-J. Lai, and Lin I, Phys. Rev. E **58**, R6947 (1998).
[12] C. Kittel, *Introduction to Solid State Physics* (Wiley, New York, 1996).
[13] G. E. Morfill and H. Thomas, J. Vac. Sci. Technol. A **14**, 490 (1996).
[14] V. A. Schweigert *et al.,* Phys. Rev. E **54**, 4155 (1996).
[15] U. Konopka, G. E. Morfill, and L. Ratke, Phys. Rev. Lett. **84**, 891 (2000).
[16] D. H. E. Dubin (private communication).